

# Complexity and anisotropy in host morphology make populations safer against epidemic outbreaks

Francisco J. Pérez-Reche<sup>1,\*</sup>, Sergei N. Taraskin<sup>2</sup>, Luciano da F. Costa<sup>3</sup>, Franco M. Neri<sup>4</sup>,  
Christopher A. Gilligan<sup>4</sup>

**1 Department of Chemistry, University of Cambridge, Cambridge, UK**

**2 St. Catharine's College and Department of Chemistry, University of Cambridge, Cambridge, UK**

**3 Institute of Physics at São Carlos, University of São Paulo, P.O. Box 369, São Carlos, São Paulo, 13560-970, Brazil, and National Institute of Science and Technology of Complex Systems, Brazil**

**4 Department of Plant Sciences, University of Cambridge, Cambridge, UK**

\* E-mail: fjp23@cam.ac.uk

## Abstract

One of the challenges in epidemiology is to account for the complex morphological structure of hosts such as plant roots, crop fields, farms, cells, animal habitats and social networks, when the transmission of infection occurs between contiguous hosts. Morphological complexity brings an inherent heterogeneity in populations and affects the dynamics of pathogen spread in such systems. We have analysed the influence of realistically complex host morphology on the threshold for invasion and epidemic outbreak in an SIR (susceptible-infected-recovered) epidemiological model. We show that disorder expressed in the host morphology and anisotropy reduces the probability of epidemic outbreak and thus makes the system more resistant to epidemic outbreaks. We obtain general analytical estimates for minimally safe bounds for an invasion threshold and then illustrate their validity by considering an example of host data for branching hosts (salamander retinal ganglion cells). Several spatial arrangements of hosts with different degrees of heterogeneity have been considered in order to analyse separately the role of shape complexity and anisotropy in the host population. The estimates for invasion threshold are linked to morphological characteristics of the hosts that can be used for determining the threshold for invasion in practical applications.

## 1 Introduction

One of the main questions in epidemiology regards the outbreak of epidemics, i.e. whether an infectious disease can spread throughout a given ensemble of hosts or not. Many systems display a threshold for epidemics which divides the parameter space into regions where an outbreak may occur from regions where the disease cannot spread (Murray, 2002; Marro & Dickman, 1999). Identification of the factors that determine such a threshold is of great importance in devising robust strategies to control the spread of disease through a population of susceptible hosts. Successful control deflects the system into the non-invasive region of parameter space so that a pathogen fails to invade. This simple concept can be applied to the spread of infection and disease, at a range of scales from the cellular, in which the host comprises a single cell, through populations of plants and animals in which a host equates with an individual organism, up to larger-scale systems, in which the unit of interest may be an individual field or farm for crop and livestock disease, a school, a village or other natural clustering for human disease. The challenge at each scale lies in dealing in a quantitative manner with factors such as stochasticity and heterogeneity, so that thresholds used to identify strategies for control are robust to these uncertainties. Stochasticity in disease spread is linked to the fact that susceptible hosts become infected only with a certain probability when challenged by inoculum from infected hosts under otherwise identical circumstances. Heterogeneity, on the

other hand, is associated with a range of factors that may differ amongst hosts. These include disorder in characteristics such as pathogen infectivity and host susceptibility, and the spatial arrangement of hosts. For certain types of hosts, heterogeneity also includes the inherent morphological complexity (i.e. irregularity in shape) of the host. Morphological complexity is especially important in epidemiological spread where it affects the contact rate between contiguous hosts. Examples of morphologically complex hosts include dendritic cells and plants, crop fields and farms, and individual clusters in social networks (Davis *et al.*, 2008; González *et al.*, 2008; Soriano *et al.*, 2008; Boender *et al.*, 2007; Eisinger & Thulke, 2008).

While the problem of disease invasion has been extensively studied, both experimentally and theoretically, most attention has been focused first on deterministic systems and increasingly on stochastic models (Murray, 2002; Truscott & Gilligan, 2003; Gibson *et al.*, 2004). Heterogeneity has traditionally received less attention although there are some remarkable exceptions (e.g. Levin & Durrett (1996); Newman (2002); Sander *et al.* (2002, 2003); Cook *et al.* (2007); Boender *et al.* (2007); Eisinger & Thulke (2008); Miller (2007); Kenah & Robins (2007); Volz (2008)). However, none of the previous work has established a link between heterogeneity and morphological features of the system leading to such a heterogeneity. In particular, the heterogeneity associated with the host morphology and the effects it may have on the features of the epidemics remain to be understood.

In systems where the pathogen is transmitted between hosts due to their proximity, one can identify three main factors that determine the invasion threshold (see Fig. 1): (i) spatial arrangement of the hosts in the population; (ii) *morphology*, i.e. the shape of the hosts, and (iii) the infection efficiency resulting from the net effect of the interplay between the pathogen infectivity and the host susceptibility upon contact.

Several models have been proposed for the dynamics of epidemics spreading by contacts between hosts (Murray, 2002; Liggett, 1985; Marro & Dickman, 1999; Hinrichsen, 2000; Ódor, 2004). In such models, the hosts can be in different states, e.g. susceptible (S), infected (I), and recovered (or removed) (R) in the prototype SIR epidemiological model. The state of each host may change according to certain model-dependent rules. For instance, the SIR model assumes that infected hosts can infect others that are susceptible and then become recovered and fully immune to further pathogen attacks. In such models, the stochasticity and heterogeneity for the spreading process are treated in a simplistic way by using phenomenological probability densities for relevant parameters and thus not linking the host morphology and invasion threshold.

In this paper, we establish a quantitative link between host morphology and the invasion threshold in an ensemble of hosts with realistically complex morphology. By analysing the conditions for epidemic outbreak in several systems with different degrees of configurational heterogeneity, we conclude that the invasion threshold is mainly determined by: (i) the average overlap between neighbouring hosts, (ii) the morphological complexity of hosts, and (iii) the host shape anisotropy. In particular, we demonstrate analytically and numerically that the resilience of the system to invasion increases with morphological complexity and anisotropy of hosts. This result is valid under very general conditions and is therefore applicable to a wide range of host ensembles. We show that irrespective of the degree of the host anisotropy the spreading process can be described in terms of a mean-field system, so that analytical estimates for the invasion threshold can be obtained. In addition, we complete our analysis by identifying several morphological characteristics that can be used for determining the threshold for invasion resulting in an epidemic outbreak.

## 2 Methods

We consider a set of  $N$  morphologically different branching structures,  $n = 1, 2, \dots, N$ , placed on all nodes  $i = 1, 2, \dots, L^2$  of an  $L \times L$  regular lattice with spacing  $a$  and nearest neighbour links only (see Table ?? for a summary of the notation used in the text). In particular, we deal with a triangular lattice

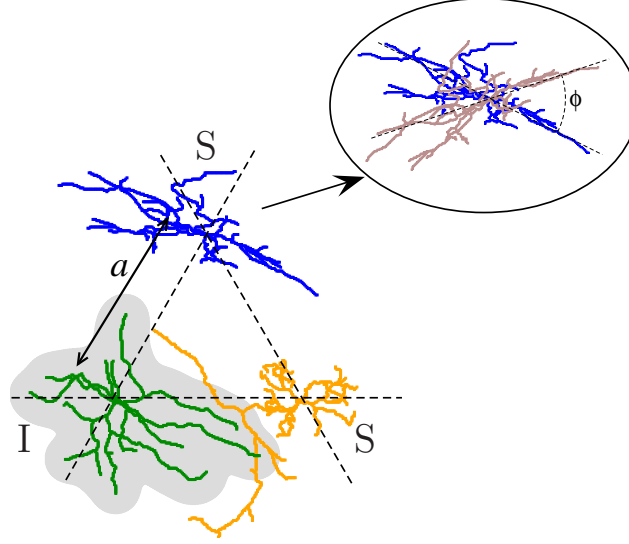


**Figure 1.** Example of a system formed by complex hosts represented, for concreteness, by planar neurons corresponding to the salamander retinal ganglion cells placed on the nodes of a triangular lattice with lattice spacing  $a$  in such a way that the somata coincide with the lattice nodes. The pathogen infests the surroundings (shaded area) of infected (I) hosts and, eventually, reaches the neighbouring susceptible hosts (e.g. amber susceptible (S) neuron on the right from I). The probability of infection of a susceptible host and the probability of a global epidemic outbreak depend on overlaps,  $J$ , between the infested region and susceptible hosts, and infection efficiency,  $k$ . The overlaps are dictated by the host morphology and spatial arrangement of hosts. The infection efficiency determines the effectiveness of the contact in terms of transmission of infection. Besides these factors, the inset shows that  $J$ , and thus the invasion threshold depend, in general, on the local orientation of the hosts,  $\phi$ .

(see Fig. 1) because this arrangement corresponds to the organisation of hosts with the highest risk of epidemic spread, in the sense that any other 2D regular lattices with the same lattice spacing is more resistant to epidemic invasion (Isichenko, 1992; Stauffer & Aharony, 1994). An additional advantage of the triangular lattice is that the next-nearest-neighbour links (ignored in our approach) are less likely in such a lattice as compared with other 2D lattices. A certain spatial configuration of generally anisotropic branching structures is fully defined in terms of the set of hosts placed on the lattice nodes,  $\{n_i\}$  (where  $n_i$  is the host number placed on node  $i$ ), and their orientations,  $\{\phi_i\}$ . The system of hosts can be either homogeneous, if morphologically identical hosts,  $n_i = n$ , of the same orientation,  $\phi_i = \phi$ , are placed on the lattice, or heterogeneous if the hosts  $n_i$  and/or their orientations  $\phi_i$  are chosen, e.g. at random. Specifically, we consider three types of arrangements with different degrees of heterogeneity which allow the various factors contributing to the invasion threshold to be analysed separately:

- \* Arrangements 1: both  $n_i$  and  $\phi_i$  are distributed according to uniform distributions so that all possible hosts and orientations are equally probable. These are highly disordered configurations.
- \* Arrangements 2: the same host is placed on all the nodes with the same orientation (i.e.,  $n_i = n$  and  $\phi_i = \phi$  for all the nodes  $i$ ). Such ordered arrangements highlight the role of the host anisotropy leading to different overlaps along different lattice directions.
- \* Arrangements 3: the same host is placed on all the nodes and its orientation is drawn from a uniform distribution of width  $\Delta\phi$  and mean value  $\bar{\phi}$ . Such arrangements allow both the morphological

complexity and anisotropy of hosts to be analysed in a comparative manner and they contain arrangements of type 2 as particular cases with  $\bar{\phi} = \phi$  and  $\Delta\phi = 0$ .

**Table 1.** Symbols and definitions used in the text. Indexes  $i$  and  $j$  span the  $L \times L$  nodes in the (triangular) lattice. Index  $\alpha$  spans the three main lattice directions, i.e.,  $\alpha = 1, 2, 3$ . Hosts are labeled by an index  $n = 1, 2, \dots, N$ . The symbol  $p_c$  stands for the bond percolation threshold.

<b>Host characteristics, arrangement, and overlaps</b>	
$\rho(\mathbf{r}; n)$	Host density
$\phi$	Host orientation
$a$	Lattice spacing
$J_{ij} = \int \rho(\mathbf{r}; n_i) \rho(\mathbf{r} - \mathbf{a}; n_j) d\mathbf{r}$	Overlap between hosts at nodes $i$ and $j$
$\mathcal{J} = \{J_{ij}\}$	Set of overlaps between all the pair of hosts
$V_1 = \frac{1}{3} \sum_{\alpha=1}^3 (\langle \mathcal{J}_\alpha^2 \rangle - \langle \mathcal{J}_\alpha \rangle^2)$	Dispersion of $\mathcal{J}$ associated with the shape complexity
$V_2 = \frac{1}{3(1+p_c)} \sum_{\alpha=1}^3 (\langle \mathcal{J}_\alpha \rangle - \langle \mathcal{J} \rangle)^2$	Dispersion of $\mathcal{J}$ associated with the shape anisotropy
<b>Disease transmission</b>	
$k$	Infection efficiency
$\tau = 1$	Recovery time
$\beta_{ij} = kJ_{ij}$	Transmission rate
$T_{ij} = 1 - e^{-\beta_{ij}\tau} = 1 - e^{-kJ_{ij}}$	Transmissibility
<b>Invasion of infection</b>	
$P_{\text{inv}}(k, a)$	Probability of invasion
$a_c(k) = \inf\{a : P_{\text{inv}}(k, a) = 0\}$	Invasion threshold in terms of the lattice spacing
$k_c(a) = \sup\{k : P_{\text{inv}}(k, a) = 0\}$	Invasion threshold in terms of the infection efficiency
$k_c^0 \propto \langle \mathcal{J} \rangle^{-1}$	Invasion threshold in a mean-field system with overlaps $\langle \mathcal{J} \rangle$
$\Delta k_1 \propto V_1$	Non-mean-field contribution to $k_c$ originated by the shape complexity
$\Delta k_2 \propto V_2$	Non-mean-field contribution to $k_c$ originated by the shape anisotropy
<b>Morphological characteristics relevant to the invasion threshold</b>	
$r^{\text{mf}}$	Radius of effective circular hosts in the mean-field approximation
$\{d_1, d_2, d_3\}, (d_1 \leq d_2 \leq d_3)$	Lattice-adapted diameters
$\text{SLAD} = d_2$	Second lattice-adapted diameter

In order to investigate the spread of epidemics in such systems, we apply the dynamical rules of the SIR formalism. Infection and hence disease can be transmitted between infected and susceptible hosts with transmission rate  $\beta$ , and infected hosts recover after a fixed time  $\tau$ . We assume that the value of  $\tau$  is time-independent, identical for all the hosts, and thus can be chosen as the time scale of the problem,  $\tau = 1$ . Such homogeneity in  $\tau$  provides a minimally safe bound for the invasion threshold (Kuulasmaa, 1982; Cox & Durrett, 1988) (see brief explanation in Appendix A).

The transmission of infection from an infected host,  $n_i$  at node  $i$ , to a susceptible nearest neighbour,  $n_j$  at node  $j$ , separated by a unit-cell vector  $\mathbf{a}$ , is a Poisson process with a transmission rate  $\beta_{ij}$ . The value of  $\beta_{ij}$  is assumed to be proportional to the overlap  $J_{ij}$  between hosts  $i$  and  $j$ , i.e.  $\beta_{ij} = kJ_{ij}$ , where  $k$  is the infection efficiency which accounts for the effectiveness of the overlap for transmission of infection. We shall set  $k$  to be identical for all the pairs of nearest neighbours. Possible variability in  $k$

can be easily incorporated into the model but it does not change the main results qualitatively.

The overlap between hosts is defined as

$$J_{ij} = \int \rho(\mathbf{r}; n_i) \rho(\mathbf{r} - \mathbf{a}; n_j) d\mathbf{r} , \quad (1)$$

in terms of the host density,

$$\rho(\mathbf{r}; n_i) = \sum_{\mathbf{p} \in n_i} \delta(\mathbf{r} - \mathbf{p}) , \quad (2)$$

where the position vector  $\mathbf{p}$  scans all the points in the host structure  $n_i$ .

One of the main quantities involved in the SIR process is the transmissibility  $T_{ij}$  defined as the probability that the pathogen is transmitted from an infected host at node  $i$  to infect a susceptible host located at node  $j$  during the life-time,  $\tau$ , of the infected node. For a Poisson process, the transmissibility is given by the following expression (Grassberger, 1983),

$$T_{ij} = 1 - e^{-\beta_{ij}\tau} = 1 - e^{-k J_{ij}} . \quad (3)$$

Therefore, the value of  $T_{ij}$  depends on the lattice spacing,  $a$ , which determines the overlap,  $J_{ij}$ , and the infection efficiency,  $k$ .

In a finite-size population, the SIR process lasts for finite time and after its termination two types of hosts, R and S, can be found in the system. The region of the recovered hosts can be mapped onto one of the clusters in the bond percolation problem by mapping the transmissibilities  $\{T_{ij}\}$  to the bond probabilities (Grassberger, 1983). According to this mapping, the probability of invasion of disease starting from a single host,  $P_{\text{inv}}(k, a)$ , is identified with the probability that this first infected host belongs to the infinite cluster of connected sites in the bond-percolation problem. The invasion threshold is formally defined as the boundary between the invasive and the non-invasive regimes characterised by  $P_{\text{inv}} > 0$  and  $P_{\text{inv}} = 0$ , respectively. This condition introduces a separatrix in the parameter space which can be given in terms of several (control) parameters of the system, such as, for example, the infection efficiency and lattice spacing. In terms of the infection efficiency, the invasion threshold is the value  $k_c = \sup\{k : P_{\text{inv}} = 0\}$  such that relatively small values of  $k \leq k_c$  correspond to non-invasive regime (i.e.,  $P_{\text{inv}} = 0$ ), while larger values,  $k > k_c$ , describe the invasive domain (i.e.,  $P_{\text{inv}} > 0$ ). Similarly, the critical lattice spacing,  $a_c = \inf\{a : P_{\text{inv}} = 0\}$ , splits the range of lattice spacings into two regions:  $a < a_c$  and  $a \geq a_c$  corresponding to invasive and non-invasive regimes, respectively. The host morphology affects implicitly (through the overlaps between hosts  $\{J_{ij}\}$ ) both  $k_c(a)$  and  $a_c(k)$ . The morphological variability of the hosts together with the heterogeneity in their arrangement makes the set  $\{J_{ij}\}$  disperse in general. The overlap can then be regarded as a random variable  $\mathcal{J}$  taking the values  $\{J_{ij}\}$ . We will describe  $\mathcal{J}$  in terms of its average,  $\langle \mathcal{J} \rangle$ , and deviations from  $\langle \mathcal{J} \rangle$  originated by its dispersion. Consequently, it is convenient to split the expression for invasion threshold into two contributions:

$$k_c = k_c^0 + \Delta k, \quad (4)$$

where  $k_c^0$  and  $\Delta k$  are associated with the average and the dispersion of  $\mathcal{J}$ , respectively. For the spatial arrangements of branching hosts considered below, the source of dispersion in the overlaps is two-fold: (i)  $V_1$ , which is due to variability arising from complexity in the shapes of different hosts for arrangements of type 1 and (ii)  $V_2$ , which is due to variability in shape anisotropy for arrangements of type 2. Correspondingly, the value of  $\Delta k$  can be split into two components, i.e.  $\Delta k = \Delta k_1 + \Delta k_2$ , where  $\Delta k_1 \propto V_1$  and  $\Delta k_2 \propto V_2$ . Both complexity and anisotropy contribute to dispersion of the overlaps for arrangements of type 3.

For numerical illustration and concreteness, in this paper we use a set of  $N$  ( $N = 51$ ) neurons (Fig. 1) corresponding to the salamander retinal ganglion cells (Ascoli, 2006), which are mostly planar, as typical representatives of complex branching structures. In this case, the vector  $\mathbf{p}$  introduced in Eq. (2) scans all

the pixels defining the digital image of each neuron. Technically, the  $\delta$ -functions in Eq. (2) are replaced by Gaussians of width comparable to the pixel size. This broadening mimics the (diffusive) spreading of the pathogen around the host. While we are not aware of documented examples of pathogen transmission in these structures, they are representative of a broad class of structures that are known to transmit virus infections (e.g. LaVail *et al.* (1997); Ehrenguber *et al.* (2002); Chen *et al.* (2007); Samuel *et al.* (2007)). The importance here is to use the published data on complex morphology to test the general methods introduced below.

### 3 Results

In this section, we analyse the invasion threshold resulting in each of the spatial arrangements listed above and propose morphological characteristics for description of the invasion threshold.

#### 3.1 Arrangements 1. $n_i$ and $\phi_i$ random

The invasion probability in host arrangements of type 1 is presented in Fig. 2. In particular, the inset shows the dependence of the probability of invasion on the infection efficiency. The value of  $P_{\text{inv}}(k)$  is zero at small values of  $k$  and becomes positive above the threshold,  $k > k_c(a)$ . As expected,  $k_c(a)$  increases with the distance between hosts (cf. the curves marked by different symbols in the inset),  $a$ , since the infection mechanism between neighbouring hosts should be more efficient in order to invade the system with larger lattice spacing. However, the curves for  $P_{\text{inv}}$  at different  $a$  collapse onto a single master curve (see Fig. 2), if plotted as a function of an alternative control parameter, the average transmissibility,  $\langle \mathcal{T} \rangle$ , which plays the same role as bond probability in the percolation problem (Sander *et al.*, 2002, 2003). This statement was first demonstrated heuristically by Sander *et al.* (2002) for SIR processes with heterogeneous transmissibility. Indeed, it is easy to go beyond heuristic arguments and prove that the statement is valid if the transmissibilities  $\{T_{ij}\}$  are *independent and self-averaging* quantities (see demonstration in Appendix B and Kuulasmaa (1982); Miller (2007); Kenah & Robins (2007) for cases in which the transmissibilities are not independent and such description is not appropriate). The collapse in Fig. 2 suggests that transmissibilities in arrangements of type 1 satisfy these conditions. In fact, the master curve defined by the collapse coincides with that obtained for the effective *homogeneous* ‘mean-field’ system with transmissibility  $\langle \mathcal{T} \rangle$  between all the nearest neighbours (see the dashed curve in Fig. 2 which is identical for all lattice spacings). This means that the heterogeneous system is equivalent to a homogeneous ‘mean-field’ one for which the invasion threshold can be determined in an efficient manner by solving the following equation,

$$\langle \mathcal{T} \rangle = p_c, \quad (5)$$

where  $p_c \simeq 0.347$  is the bond percolation threshold in an infinite (i.e.,  $L \rightarrow \infty$ ) triangular lattice (Isichenko, 1992; Stauffer & Aharony, 1994). The value of  $p_c$  provides the minimally safe bound for invasion threshold in other 2D lattices (Isichenko, 1992; Stauffer & Aharony, 1994). Since the average  $\langle \mathcal{T} \rangle$  converges very fast with  $L$  to its limiting value for  $L \rightarrow \infty$ , the value of  $k_c(a)$  estimated from Eq. (5) is representative for macroscopic systems. The dependence of infection efficiency on lattice spacing defines the phase boundary in the  $(k, a)$  plane (see solid circles in Fig. 3(a)) between the invasive and non-invasive regimes. The threshold  $a_c(k)$  provides the same separatrix.

The influence of the host morphology on the invasion threshold can be better understood by analysing the dependence of  $k_c$  on the overlaps  $\mathcal{J}$ . The first term in Eq. (4) can be found by solving Eq. (5) for the homogeneous system in which all the overlaps are replaced by its mean value,  $\langle \mathcal{J} \rangle$ , i.e.

$$k_c^0 = \frac{|\ln(1 - p_c)|}{\langle \mathcal{J} \rangle}. \quad (6)$$

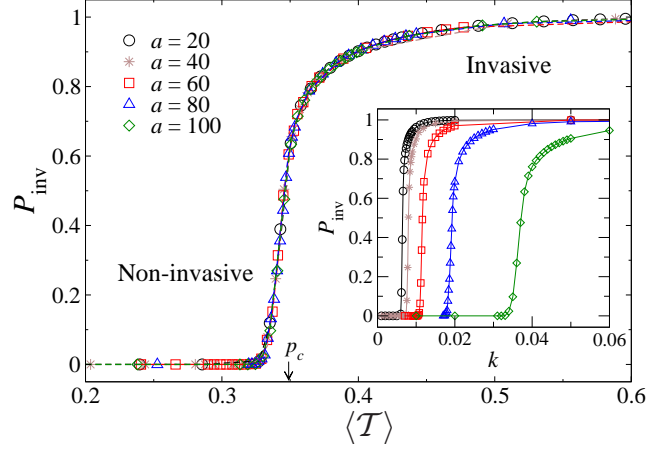


**Figure 2.** Probability of invasion,  $P_{\text{inv}}$ , for morphologically complex hosts in disordered arrangements of type 1 on a lattice of size  $L \times L = 200 \times 200$ . The main plot displays  $P_{\text{inv}}$  as a function of the average transmissibility,  $\langle \mathcal{T} \rangle$ , for heterogeneous systems with different lattice spacings  $a$  (marked by different symbols) and for a mean-field system with homogeneous transmissibility  $\langle \mathcal{T} \rangle$  (dashed line). The bond-percolation critical probability,  $p_c$ , marked by arrow gives the invasion threshold in the thermodynamic limit. The inset shows the invasion probability as a function of the infection efficiency  $k$  for different values of lattice spacing marked by the same symbols as in the main figure.

It can be rigorously shown that the value of  $k_c^0$  underestimates the threshold, i.e.  $k_c \geq k_c^0$  (cf. circles and dashed line in Fig. 3(b)). To prove this inequality we write the expression (5) in terms of the overlap as  $1 - \langle e^{-k_c \mathcal{J}} \rangle = p_c$ . Applying then the general inequality  $\langle e^{-k_c \mathcal{J}} \rangle \geq e^{-k_c \langle \mathcal{J} \rangle}$  to the above relation we obtain  $k_c \geq -\ln(1 - p_c) / \langle \mathcal{J} \rangle$  which reduces to  $k_c \geq k_c^0$  after using the expression (6) for  $k_c^0$ . This inequality implies that the contribution  $\Delta k$  to  $k_c$  associated with the dispersion of the overlaps makes systems more resilient to epidemic invasion. An approximate solution of Eq. (5) obtained by keeping the first correction to  $k_c^0$  gives the low-bound estimate  $\Delta k_1$  of  $\Delta k$ , i.e.

$$\Delta k \gtrsim \Delta k_1 = \frac{(k_c^0)^2}{2\langle \mathcal{J} \rangle} V_1, \quad (7)$$

which is proportional to the variance of the overlaps,  $V_1 = \langle \mathcal{J}^2 \rangle - \langle \mathcal{J} \rangle^2$ , with other central moments of higher order being dropped (see the derivation of Eq. (7) in Appendix D). The upper inset in Fig. 3 shows that the value of  $V_1$  is non-zero, as expected from the comparison of  $k_c$  and  $k_c^0$  plotted in the main figure.

The low-bound estimate of  $\Delta k$  given by Eq. (7) provides a safe threshold,  $k_c^0 + \Delta k_1$ , for the actual system. We expect this to be the case for a wide class of morphologically complex hosts so that describing  $\mathcal{J}$  in terms of its average and standard deviation provides a minimally safe bound to the invasion threshold in heterogeneous arrangements.

### 3.2 Arrangements 2. Identical $n_i$ and $\phi_i$ at all the nodes

In ordered arrangements of type 2, all the hosts are identical branching structures with the same orientation. The host overlaps along the main lattice directions,  $\{J_1, J_2, J_3\}$  (see Figs. 4(a)), depend on the lattice spacing  $a$ , the host used as a motif,  $n$ , and its orientation,  $\phi$ . For a given  $n$ , the set of all possible overlaps obtained by varying  $a$  and  $\phi$  within their respective domains define the host *overlap*

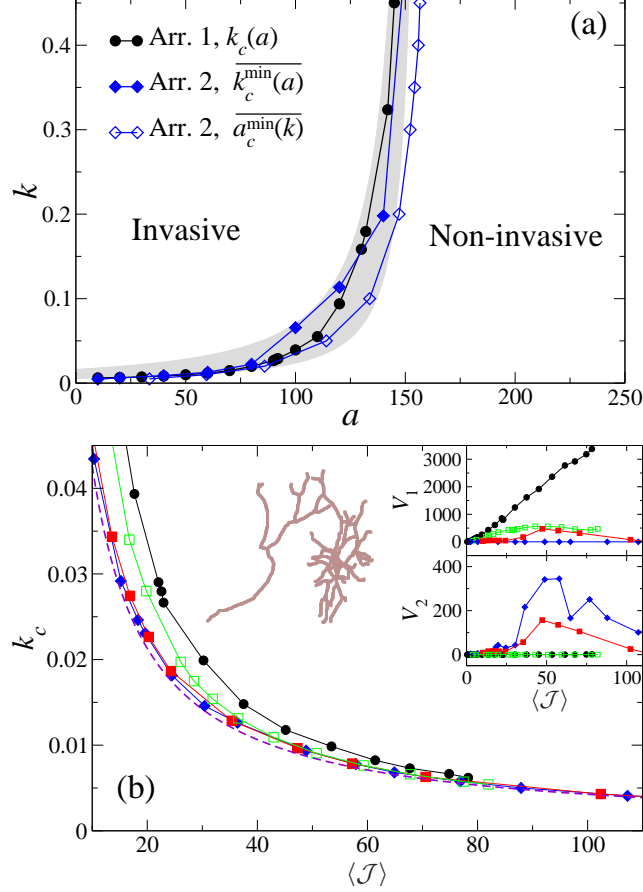


**Figure 3.** Invasion threshold for the system of branching hosts. (a) Representation in terms of the infection efficiency,  $k$ , and the lattice spacing,  $a$ . The threshold  $k_c(a)$  for arrangements of type 1 is shown by circles. The shaded region corresponds to the statistically possible values for the estimation of  $k_c(a)$  in terms of effective circular hosts with homogeneous overlaps defined in Eq. (14). Diamonds indicate the *average* thresholds  $\overline{k_c(a)}$  (solid symbols) and  $\overline{a_c(k)}$  (open symbols) for arrangements of type 3. (b) Invasion threshold  $k_c$  as a function of the average overlap  $\langle \mathcal{J} \rangle$  for arrangements of type 1 (circles), type 2 with orientation  $\phi = 0$  (diamonds) and type 3 with mean orientation  $\bar{\phi} = 0$  and two widths of uniform distribution,  $\Delta\phi = 1$  (solid squares) and  $\Delta\phi = 2\pi$  (open squares). The branching host used as a motif for arrangements of type 2 and 3 is displayed in the figure. The dashed line represents the dependence of  $k_c^0$  vs  $\langle \mathcal{J} \rangle$  given by Eq. (6). The insets show the dispersions  $V_1$  and  $V_2$  of the overlaps associated with the disorder and anisotropy, respectively, corresponding to the same arrangements as in the main figure (the symbol code is the same as in the main figure).

*locus*. Fig. 4(b) shows the overlap locus corresponding to a typical branching host displayed in Fig. 4(a). Each configuration with given  $a$  and  $\phi$  is represented by a point  $(J_1(a, \phi), J_2(a, \phi), J_3(a, \phi))$  belonging to the overlap locus. The inherent anisotropy of the host is reflected in the dispersion of the overlaps,  $J_1 \neq J_2 \neq J_3 \neq J_1$ , and gives rise to a significant deviation of the overlap locus (surface in blue) from the straight line (in black) corresponding to the locus for isotropic host ( $J_1 = J_2 = J_3$ ).

Similarly to arrangements of type 1, the spread of disease in ordered arrangements can be mapped onto the bond percolation problem but now with anisotropic bond probabilities corresponding to the values of transmissibilities,  $T_1 \neq T_2 \neq T_3 \neq T_1$ , along the main lattice directions defined as  $T_i = 1 - e^{-k J_i}$  for  $i = 1, 2, 3$ . From this mapping, the invasion threshold is defined by the following condition (Sykes & Essam, 1964),

$$1 - T_1 - T_2 - T_3 + T_1 T_2 T_3 = 0. \quad (8)$$

This condition can be recast in terms of the infection efficiency and overlaps, as  $g(J_1, J_2, J_3, k_c) = 0$ , where

$$g(J_1, J_2, J_3, k) = 1 - e^{-k(J_1+J_2)} - e^{-k(J_1+J_3)} - e^{-k(J_2+J_3)} + e^{-k(J_1+J_2+J_3)}. \quad (9)$$

For given value of  $k$ , the condition  $g = 0$  defines a critical surface (in red in Fig. 4(b)) in the overlap space. Therefore, the intersection of the critical surface with the overlap locus (in blue) defines the invasion threshold,  $a_c(k, \phi)$ . On the other hand, for a given value of  $a$  and  $\phi$ , the critical infection efficiency  $k_c(a, \phi)$  is given by the value of  $k$  which generates a critical surface containing the point  $(J_1(a, \phi), J_2(a, \phi), J_3(a, \phi))$ .

In practice, it is useful to consider the minimally resilient thresholds  $k_c^{\min}(a) = \min_{\phi} \{k_c(a, \phi)\}$  or  $a_c^{\max}(k) = \max_{\phi} \{a_c(k, \phi)\}$  which ensure that the system is safe for any orientation if  $k < k_c^{\min}(a)$  or  $a > a_c^{\max}(k)$ , respectively. The invasion thresholds are host-dependent and define different separatrices in the  $(a, k)$  plane for each host. Fig. 3(a) shows the average thresholds  $\overline{k_c^{\min}(a)}$  and  $\overline{a_c^{\max}(k)}$  over all the branching hosts  $\{n\}$ . The phase boundary,  $\overline{a_c^{\max}(k)}$ , gives the safest estimate for the invasion threshold, which is a consequence of the multivalued nature of  $a_c(k, \phi)$  in contrast to single-valued function  $k_c(a, \phi)$  (see Appendix C for more detail).

The effects of the host anisotropy on the invasion threshold can be analysed in a similar way as for configurations of type 1 by investigating the dependence of  $k_c$  on the overlaps. Similarly, the critical infection efficiency, is given by Eq. (4) with the mean-field value  $k_c^0$  evaluated for the system with mean overlap  $\langle \mathcal{J} \rangle = (J_1 + J_2 + J_3)/3$ . The dispersion in the overlaps results in the following approximate expression for  $\Delta k$  (see detailed derivation in Appendix D),

$$\Delta k \gtrsim \Delta k_2 = \frac{(k_c^0)^2}{2\langle \mathcal{J} \rangle} V_2, \quad (10)$$

where the quantity  $V_2 = \frac{1}{3(1+p_c)} \sum_{\alpha=1}^3 (J_{\alpha} - \langle \mathcal{J} \rangle)^2$  accounts for the anisotropy of the overlaps. The value of  $\Delta k_2$  is non-negative meaning that  $k_c \geq k_c^0$ , i.e. the anisotropy in host shape makes the system more resilient as compared with the system of isotropic hosts with the same mean overlap.

As an example, Fig. 3(b) shows that  $k_c > k_c^0$  in the system of branching hosts, in agreement with the predicted behaviour (cf. diamonds and the dashed line). The inset shows the corresponding dispersion  $V_2$ . Given that the deviation of  $k_c$  from  $k_c^0$  is small in the system of branching hosts considered, the correction  $\Delta k_2$  is in fact a good approximation to the actual deviation  $\Delta k$ . This is the expected behaviour for systems of hosts with moderate anisotropy.

### 3.3 Arrangements 3. Identical $n_i$ and random $\phi_i$

In the two previous sections, it has been shown that both the disorder and anisotropy of the hosts make systems of branching hosts more resilient against epidemics. The arrangements of type 1 and 2 are

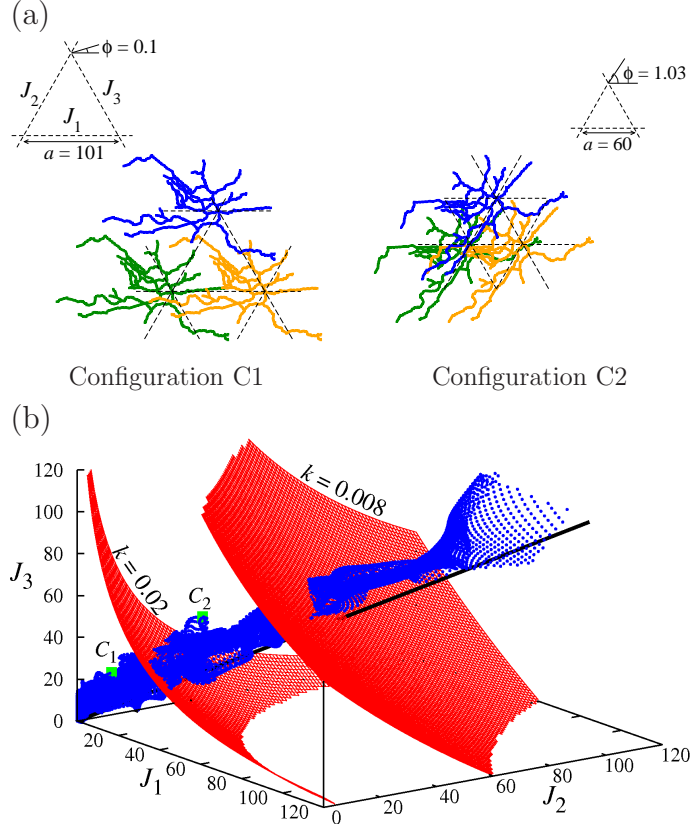


**Figure 4.** Arrangements of type 2 (an identical host with the same orientation placed at all the nodes). (a) Unit cell of two different configurations constructed by using the same branching host. The orientation,  $\phi$ , and spacing,  $a$ , corresponding to each case are indicated in the schematic reference frames displayed at the top. As shown in the left frame, there are three different values of the overlaps,  $\{J_1, J_2, J_3\}$ , corresponding to each of the main directions in the lattice. (b) Space of overlaps,  $(J_1, J_2, J_3)$ . Each configuration with different  $a$  and  $\phi$  is mapped into a point in this space. The set of overlaps corresponding to all the possible configurations obtained for a given host defines its overlap locus (surface in blue). The deviation of the blue surface from the straight black line representing overlaps between isotropic hosts ( $J_1 = J_2 = J_3$ ) shows the degree of anisotropy in the overlaps for a typical branching host (shown in (a)). High values of the overlaps correspond to small lattice spacings  $a$ . In particular, the points labeled as C1 and C2 correspond to the configurations shown in (a). The critical surface defined by  $g(J_1, J_2, J_3, k) = 0$  (see Eq. (9)) is shown in red for two values of the infection efficiency:  $k = 0.02$  and  $k = 0.008$ . For a given value of  $k$ , the points in the overlap locus below/above the critical surface correspond to safe/vulnerable configurations. The intersection of the overlap locus with the critical surfaces parameterized by  $k$  determines the critical threshold  $a_c(k, \phi)$ . The critical infection efficiency  $k_c(a, \phi)$  corresponding to a configuration with lattice spacing  $a$  and orientation  $\phi$  is given by the value of  $k$  related to the critical surface containing the configuration point  $\{J_1(a, \phi), J_2(a, \phi), J_3(a, \phi)\}$ .

extreme cases in the sense that the first type highlights the morphological complexity ( $V_1 \geq 0$  and  $V_2 = 0$ ) whereas the second type highlights the effects of the anisotropy of the hosts ( $V_1 = 0$  and  $V_2 \geq 0$ ). In generic arrangements, such as those of the type 3 defined above, the two effects are present. By assuming that the transmissibilities between different pairs of hosts are independent, it is possible to show that the behaviour of the actual heterogeneous system is equivalent to that of a mean-field *homogeneous* system with anisotropic transmissibilities  $\{\langle \mathcal{T}_1 \rangle, \langle \mathcal{T}_2 \rangle, \langle \mathcal{T}_3 \rangle\}$ , where  $\langle \mathcal{T}_\alpha \rangle$  is the average of the transmissibility along the direction  $\alpha$  in the lattice. A proof for this statement, which represents a generalisation to systems with anisotropic transmissibilities of the mean-field description suggested in Sander *et al.* (2002, 2003), is given in Appendix B. The equation for the invasion threshold in this case is

$$1 - \langle \mathcal{T}_1 \rangle - \langle \mathcal{T}_2 \rangle - \langle \mathcal{T}_3 \rangle + \langle \mathcal{T}_1 \rangle \langle \mathcal{T}_2 \rangle \langle \mathcal{T}_3 \rangle = 0, \quad (11)$$

which generalises the formulae (5) and (8) in such a way that Eq. (5) corresponds to the particular case of Eq. (11) when  $\langle \mathcal{T} \rangle$  is the same along all the directions and Eq. (8) emerges when there is no disorder in the anisotropic transmissibilities.

As for the previous arrangements, the critical infection efficiency obeys Eq. (4) with both heterogeneity and anisotropy contributing to  $\Delta k$ . The lowest-order approximation to the lower bound for  $\Delta k$  is given by the relation  $\Delta k \gtrsim \Delta k_3 = \Delta k_1 + \Delta k_2$  (see details in Appendix D) where  $\Delta k_1$  and  $\Delta k_2$  are defined in Eqs. (7) and (10), respectively, with the dispersions terms generalised to

$$V_1 = \frac{1}{3} \sum_{\alpha=1}^3 (\langle \mathcal{J}_\alpha^2 \rangle - \langle \mathcal{J}_\alpha \rangle^2), \quad (12)$$

$$V_2 = \frac{1}{3(1+p_c)} \sum_{\alpha=1}^3 (\langle \mathcal{J}_\alpha \rangle - \langle \mathcal{J} \rangle)^2. \quad (13)$$

Fig. 3(b) shows that the increase in orientational variability  $\Delta\phi$  brings additional heterogeneity in the system and thus results in a decrease of  $V_2$  but this does not necessarily induce a decrease in the value of critical infection efficiency since the contribution  $V_1$  may increase. This illustrates the interplay between the role of disorder and host anisotropy.

### 3.4 Description of the invasion threshold in terms of morphological characteristics

In the previous sections, we have established a link between the invasion threshold and host overlaps  $\mathcal{J}$  characterised by the first moment,  $\langle \mathcal{J} \rangle$ , and the deviations from the mean,  $V_1$  and  $V_2$ . The missing link between the host morphology and invasion threshold can be recovered by studying how the morphology affects overlaps. Here we show that both  $\langle \mathcal{J} \rangle$  and the anisotropy of  $\mathcal{J}$  (i.e.  $V_2$ ) can be well described in terms of a reduced number of morphological characteristics. In contrast, a proper description of the disorder-induced contribution from  $\Delta k_1$  in terms of a reasonably small set of morphological characteristics is hardly possible and requires instead knowledge of the spatial host density,  $\rho(\mathbf{r})$  (see Eq. (2)). However, we can ignore the disorder-induced contributions from  $\Delta k_1$  in order to obtain a safe lower bound for critical infection efficiency and thus connect this quantity with morphological characteristics of hosts.

We start the analysis by considering arrangements of type 1. The overlaps  $\mathcal{J}$  are statistically isotropic (i.e.,  $V_2 = 0$ , Fig. 3(b)) so that the invasion threshold can be described in terms of a mean-field system with *homogeneous* and *isotropic* overlaps,  $\mathcal{J}^{\text{mf}}$ , and corresponding transmissibilities  $\langle \mathcal{T} \rangle$ . The mean-field system consists of effective circular hosts of radius  $r^{\text{mf}}$  with overlap  $\mathcal{J}^{\text{mf}}$ . These effective circles are fully described by the radius,  $r^{\text{mf}}$ , and density,  $\rho^{\text{mf}}(r)$ , which is positive for  $0 < r \leq r^{\text{mf}}$  and is zero otherwise. The functional form of  $\rho^{\text{mf}}(r)$  is the same as of real branching hosts in  $[0, r^{\text{mf}}]$ , i.e.  $\rho(r) \propto r^{d_f-2}$  where  $d_f$  stands for the fractal dimension (see Appendix E for more detail). The radius of the effective circles

is defined as  $r^{\text{mf}} = \frac{d_f+1}{d_f} \langle r \rangle$  to ensure that the average radius of the effective circles coincides with the average radius of the actual hosts,  $\langle r \rangle$  (see Appendix E). Under these assumptions, the expression for the overlap between neighbouring effective circles is given by

$$\langle \mathcal{J} \rangle \simeq \mathcal{J}^{\text{mf}} \simeq \frac{1}{3} \left( \frac{M d_f}{\pi a} \right)^2 \left( \frac{r^{\text{mf}}}{a} \right)^{-7/2} \left( \frac{2r^{\text{mf}}}{a} - 1 \right)^{3/2}, \quad (14)$$

valid for small overlaps when  $2r^{\text{mf}}/a - 1 \ll 1$ . The parameter  $M$  is a normalisation constant (see Appendix E). The substitution of this expression for  $\langle \mathcal{J} \rangle$  into Eq. (6) gives the required link between the invasion threshold and the effective radius,  $k_c^{\text{mf}} \propto (r^{\text{mf}}/a)^{7/2} (2r^{\text{mf}}/a - 1)^{-3/2}$ . In fact, for the particular system of branching hosts studied here, this is a very good estimate for the value of the critical infection efficiency,  $k_c \gtrsim k_c^{\text{mf}}$ , as demonstrated in Fig. 3 (the solid circled line falls inside the shaded gray area representing the set of possible values for  $k_c^{\text{mf}}$  within statistical errors). This means that for the arrangements of type 1, the mean-field homogeneous system of effective circles can be reliably used for estimating the phase boundaries.

In the case of ordered (type 2) and partially ordered (type 3) arrangements, the overlaps along distinct lattice directions can be significantly different and thus crucial for evaluation of the invasion threshold in contrast to the mean overlap which is important for disordered (mean-field like) arrangements of type 1. Therefore, instead of a single characteristic such as mean radius of the effective circles for disordered arrangements, we introduce an ordered set of linear sizes of branching hosts along the lattice directions, i.e the set of lattice-adapted diameters,  $\{d_1, d_2, d_3\}$  ( $d_1 \leq d_2 \leq d_3$ ; see illustration in Fig. 5). The second lattice-adapted diameter (SLAD),  $d_2$ , plays the most important role for finding the critical value of, e.g. lattice spacing, and thus estimating the invasion threshold. This is due to the fact that Eqs. (8) and (11) have a solution for the critical threshold only if the overlaps at least along two directions are finite. The overlaps become greater than zero if the lattice-adapted diameters are comparable or greater than the lattice spacing and thus solution of Eqs. (8) and (11) exists if  $a \lesssim d_2$ . This qualitative analysis suggests the existence of strong correlations between the SLAD and  $a_c$ . Indeed, we have observed such correlations, i.e.  $a_c \simeq d_2$ , for ordered arrangements of type 2 (see Fig. 5). The description of  $a_c$  in terms of SLAD gets worse for small values of  $k$  (see the black squares in Fig. 5) when the strong overlaps between hosts should be achieved at criticality and thus the interior density of the hosts, rather than the diameter only, becomes important.

## 4 Discussion and Conclusions

Using the framework of an SIR epidemiological model, we have investigated the transmission of infection and spread of disease in systems of hosts with realistically complex morphology. Our main finding is that the greater the irregularity in the host morphology, the more resilient is the population to epidemic invasion under otherwise identical conditions (for instance, identical spatial arrangement of hosts). We derive a safe lower bound for the invasion threshold, which has been obtained for branching hosts with independent transmission rates placed on a triangular lattice. We have shown mathematically that this bound holds for all other 2-D topological arrangements of hosts with nearest-neighbour transmission and even in the case when the transmission rates between different hosts are correlated with each other. In particular, irregularity in the host positions, i.e. small random displacements of hosts from lattice nodes bring correlations in transmissibilities and thus make the system more resilient. Of course, for some real systems, the assumption about nearest-neighbor transmission may be violated by the presence of short-cuts between remote nodes due, for example, to wind or animal motion. In this case, it is known that the system becomes less resilient to epidemic invasion (Sander *et al.*, 2002) and the bounds given above are no longer valid.

We have used a set of planar neurons to illustrate the effects of complex branching hosts on the spread of infection. We have identified two sources of heterogeneity in the systems considered: (i) morphological

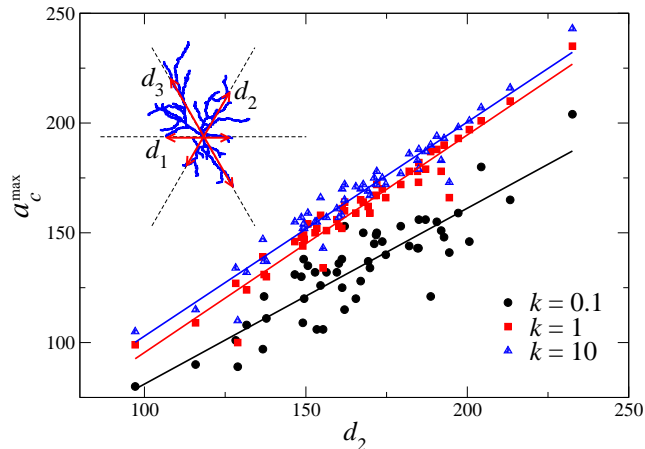


**Figure 5.** Dependence of the critical lattice spacing,  $a_c^{\max}(k)$  on the SLAD,  $d_2$ , for all the branching hosts in arrangements of type 2. Different symbols refer to different values of  $k$  as marked and each point for a particular symbol corresponds to an individual branching host. The solid lines represent the linear regression fit for each value of  $k$  (e.g.  $a_c(k) = 14.1 + 0.94d_2$  with correlation coefficient  $\simeq 0.97$  for  $k = 1$ ). The inset defines graphically the lattice-adapted diameters  $\{d_1, d_2, d_3\}$ .

complexity of hosts and (ii) the host shape anisotropy. Both contribute to the resilience of the system against epidemic invasion and can be described by means of two morphological characteristics of hosts, i.e. by the mean effective radius and the second lattice-adapted diameter. Such characterisation is not exact in general but it provides a safe bound to the invasion threshold. The main conclusions are generic and remain valid for any type of morphologically complex hosts. In particular, the methodology introduced here and the bounds for resilience to invasion apply to the transmission of infection in other 2-D systems with analogous disorder expressed in the host morphology and anisotropy. Examples include the spread of plant disease through contacts between adjacent plants in a field, orchard or forest in which the host plants frequently occur on a 2-D lattice. Here the contact structures between nearest-neighbours are determined by overlap of shoots (for aerial pathogens) or roots (for soil-borne pathogens) (Gilligan, 2008) in which the 3-D structure of the plant can be collapsed onto a 2-D framework when considering transmission of infection between nearest-neighbours. In principle, a similar analysis could be performed for ensembles of morphologically complex 3-D hosts arranged on a 2-D lattice that takes explicit account of the three dimensional host structure. Expressions for the invasion threshold are not known analytically in this case and the precise definition of quantities directly linked to host morphologies such as fractal dimensions or average radius are system-dependent that require further study. Other potential applications of the methods include analysis of the transmission of infection via the ‘morphology’ of contacts between clusters of susceptible hosts in social networks, in which the clusters can be approximated by a 2-D lattice (cf recent work on percolation models for the spread of plague through gerbil populations in lattices of interconnecting burrows (Davis *et al.*, 2008)).

The present work opens several possible directions of further research for practical applications in considering disease control strategies and for basic understanding of epidemic spread involving heterogeneous transmission of infection. For instance, our analysis suggests new ways for control of epidemics in real systems where host morphology is inherently complex. For example, in a system where an epidemic is active, a treatment enhancing the anisotropy in the transmission rates, would be more efficient as compared with reduction of transmission rates in all directions, i.e. isotropically. Such might arise with the deployment of microbiological biological control agents to restrict the spread of infection of soil-borne

pathogens in plant populations (Gibson *et al.*, 1999). Biological control agents often exhibit marked variability in performance (Gibson *et al.*, 1999), failing to provide isotropic control of infection on targeted hosts, for example due to uneven colonization of roots by microbial antagonists deployed as biological control agents. Our results suggest that increasing the degree of anisotropy due to these organisms may yet contribute to success in controlling invasion. Anisotropy may also be fostered in social or animal systems by preferential treatment of some, rather than all, connections between clusters. The findings in the current manuscript are also important for better understanding virus tracing of neurons (e.g. Loewy (1998)), which is a biological staining method where virus propagation from neuron to neuron is used as a means to histologically mark the interconnections, so that they become visible to the microscope. More specifically, our results imply that virus tracing might be not so effective in the case of anisotropic or not so complex neuronal cells, which could therefore be overlooked by this type of marking. Analogue effects can be also important in transneuronal spreading of virus in order to deliver gene therapy (Oztas, 2003).

Finally, the approach presented here is relevant to epidemics for which an SIR model is suitable and a mapping to ordinary percolation exists. While many diseases can be described by the SIR framework, others cannot. It would be interesting to analyze the effect of host morphology within the framework of a different family of epidemiological models with final state not immune to the disease (such as the susceptible-infected-susceptible model). Such an extension is challenging since the mapping to ordinary percolation is no longer possible requiring tools such as directed percolation (Marro & Dickman, 1999; Hinrichsen, 2000) from non-equilibrium physics.

## Appendices

### A Homogeneous recovery times

In the present work, we have assumed that the recovery times of the hosts are homogeneous. This assumption provides a minimally safe bound for the invasion threshold for epidemic outbreak so that the systems with disorder in  $\tau$  are safer i.e. less likely to be invaded. Indeed, the probability of invasion  $P_{\text{inv}}^{\mathcal{A}}$  in an SIR process  $\mathcal{A}$  with heterogeneous  $\tau$  and average transmissibility  $\langle \mathcal{T} \rangle$  satisfies (Kuulasmaa, 1982; Cox & Durrett, 1988):

$$P_{\text{inv}}^{\mathcal{A}} \leq P_{\text{inv}}^{\mathcal{B}}, \quad (15)$$

where  $P_{\text{inv}}^{\mathcal{B}}$  is the probability of invasion in an SIR process  $\mathcal{B}$  with the same average transmissibility as in  $\mathcal{A}$  but with homogeneous  $\tau$ . The above inequality implies that the non-invasive region for the heterogeneous (in  $\tau$ ) system is wider than for the homogeneous one.

### B Validity of the mean-field description of heterogeneous systems

The validity of the mean-field description leading to the threshold condition (2) in the main text in systems with isotropic disorder was heuristically suggested by Sander *et al.* (2002). In fact, it can be proven more generally that *the mean-field description is valid both in the presence of isotropic and anisotropic uncorrelated disorder provided the overlaps between different pairs of hosts (and thus transmissibilities) are self-averaging independent quantities*<sup>1</sup>. In order to prove this, let us interpret  $T_{ij}$  as the conditional probability,  $T_{ij}(J) = P(i \rightarrow j|J)$ , for infection to be transmitted from host  $i$  to host  $j$  given the overlap  $J$  which is a random variable. In the anisotropic case, the overlaps along different lattice directions are distributed according to distinct and independent probability densities, e.g.,  $\{f_{\alpha}(J), \alpha = 1, 2, 3\}$  for a

---

<sup>1</sup>A physical characteristic of a disordered system is said to be self-averaging if its average over several configurations of disorder coincides with its average in a single infinitely large configuration (Sornette, 2000).

triangular lattice. The probability that the disease is transmitted from an infected host at node  $i$  to one of its neighbors at node  $j$  along the direction  $\alpha$  is given then by the following expression,

$$\langle T_{ij}^{(\alpha)} \rangle = \int_J T_{ij}(J) f_\alpha(J) dJ \quad (16)$$

which is identical for all the pairs  $(i, j)$  along direction  $\alpha$  and thus coincides with the average transmissibility  $\langle \mathcal{T}_\alpha \rangle \equiv \langle T_{ij}^{(\alpha)} \rangle$  if the transmissibility is a self-averaging quantity. We have checked that the self-averaging condition indeed holds for branching structures by demonstrating that the probability of invasion does not depend on the particular configuration of hosts. This is illustrated in Fig. 6 where we show that the invasion probability curves ( $P_{\text{inv}}$  vs  $\langle \mathcal{T} \rangle$ ) collapse for different realizations of disorder.

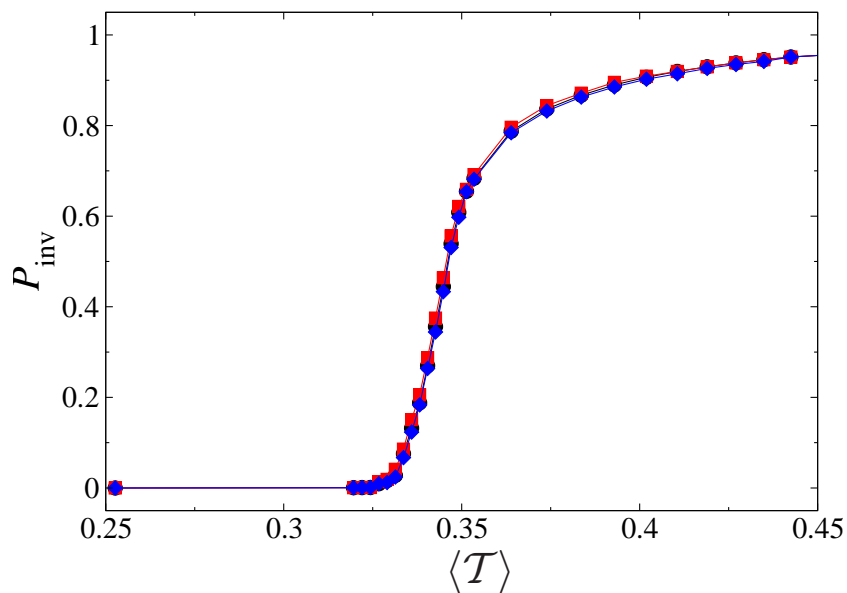


**Figure 6.** Probability of invasion,  $P_{\text{inv}}$ , for arrangement of type 1 (system size  $L \times L = 200 \times 200$ ) with lattice spacing  $a = 80$ . Different symbols (squares, circles, and diamonds) correspond to three different configurations of hosts.

As a consequence of the above analysis, the system can be mapped onto an anisotropic but homogeneous mean-field system with transmissibilities,  $\{\langle \mathcal{T}_\alpha \rangle\}$ . Therefore, Eq. (8, main text) giving the invasion threshold for an anisotropic disordered system can be obtained from Eq. (5, main text) by replacing the anisotropic transmissibilities  $\{T_\alpha\}$  by the mean values  $\{\langle \mathcal{T}_\alpha \rangle\}$ . In the particular case of isotropic triangular system,  $\langle \mathcal{T}_\alpha \rangle = \langle \mathcal{T} \rangle$ , so that Eq. (8, main text) reduces to  $1 - 3\langle \mathcal{T} \rangle + \langle \mathcal{T} \rangle^3 = 0$  which has the solution  $\langle \mathcal{T} \rangle = p_c$ , where  $p_c = 2 \sin(\pi/18) \simeq 0.347$  (Isichenko, 1992; Stauffer & Aharony, 1994).

## C Multivalued behaviour of critical lattice spacing

The invasion threshold in the ordered arrangements of type 2 (the same host is placed on all the nodes with the same orientation,  $\phi$ ) is given by the condition  $g = 0$  (see Eq. (6) in the main text). The function  $g$  depends on the overlaps along the main lattice directions,  $\{J_\alpha(a, \phi), \alpha = 1, 2, 3\}$ . For fixed orientation  $\phi$ , the overlap  $J_\alpha(a, \phi)$  between branching structures is generally a non-monotonic function of

the lattice spacing (see blue and red curves in the inset in Fig. 7). In this figure, we show that the non-monotonic character of the overlaps results in non-monotonic behaviour of the critical infection efficiency,  $k_c(a, \phi)$ , and confers a multivaluated dependence of the critical lattice spacing,  $a_c(k, \phi)$  versus  $k$ . As a consequence, the minimally resilient threshold in terms of the lattice spacing,  $a_c^{\max}(k) = \max_{\phi} \{a_c(k, \phi)\}$  (see the illustration for  $a_c^{\max}(k)$  in Fig. 7 where this quantity is represented by the red curve) gives a safer boundary as compared to the minimally resilient threshold in terms of the infection efficiency,  $k_c^{\min}(a) = \min_{\phi} \{k_c(a, \phi)\}$  (the black curve), i.e. the red curve in Fig. 7 either coincides with or is to the right of the black one.

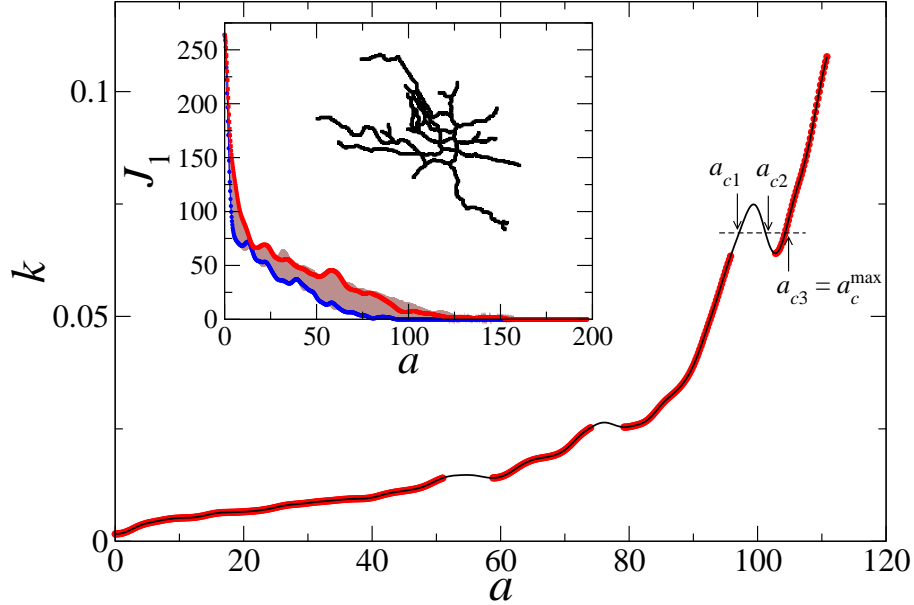


**Figure 7.** Infection efficiency versus lattice spacing for fixed orientation of branching hosts represented by a planar neuron shown in the inset. The definition of the maximally resilient threshold  $a_c^{\max}(k)$  (red curve) is illustrated for a particular value of  $k$  for which  $a_c(k, \phi)$  takes three different values. The inset shows the dependence  $J_1(a)$  along one of the lattice directions for the arrangement of type 2 obtained by using the displayed host as a motif. The shaded (brown) region indicates the overlaps for all the possible orientations,  $\phi$ , of the host. Blue and red lines correspond to  $J_1(a)$  for  $\phi = 0$  and  $\phi = 1$ , respectively.

## D Analytical estimates for the invasion threshold

In this Section, we derive an approximate analytical expression for  $k_c$  for arrangements of type 3 and extend this result to other arrangements.

We start from Eq. (8) in the main text which is valid for arrangements of type 3. Expressing the transmissibilities,  $\{\mathcal{T}_\alpha, \alpha = 1, 2, 3\}$ , in terms of anisotropic overlaps,  $\{\mathcal{J}_\alpha, \alpha = 1, 2, 3\}$ , gives

$$1 - \langle e^{-k_c \mathcal{J}_1} \rangle \langle e^{-k_c \mathcal{J}_2} \rangle - \langle e^{-k_c \mathcal{J}_1} \rangle \langle e^{-k_c \mathcal{J}_3} \rangle - \langle e^{-k_c \mathcal{J}_2} \rangle \langle e^{-k_c \mathcal{J}_3} \rangle + \langle e^{-k_c \mathcal{J}_1} \rangle \langle e^{-k_c \mathcal{J}_2} \rangle \langle e^{-k_c \mathcal{J}_3} \rangle = 0. \quad (17)$$

The overlaps,  $\mathcal{J}_\alpha = \langle \mathcal{J}_\alpha \rangle + \delta \mathcal{J}_\alpha$ , along lattice direction  $\alpha$  are random values characterized by the mean value  $\langle \mathcal{J}_\alpha \rangle$  and deviations from the mean,  $\delta \mathcal{J}_\alpha$ . Anisotropy brings an additional source of dispersion,  $\Delta \mathcal{J}_\alpha = \langle \mathcal{J}_\alpha \rangle - \langle \mathcal{J} \rangle$ , where the overall mean overlap is  $\langle \mathcal{J} \rangle = \frac{1}{3} \sum_{\alpha=1}^3 \langle \mathcal{J}_\alpha \rangle$ . Expanding Eq. (17) in small

$\delta\mathcal{J}_\alpha \ll \langle\mathcal{J}_\alpha\rangle$  first and then in  $\Delta\mathcal{J}_\alpha \ll \langle\mathcal{J}\rangle$  and keeping the leading corrections to the the mean-field value, results in the following expression:

$$1 - 3e^{-2k_c\langle\mathcal{J}\rangle} + e^{-3k_c\langle\mathcal{J}\rangle} + \left[ \left( \frac{e^{-k_c\langle\mathcal{J}\rangle}}{2} - 1 \right) \sum_{\alpha=1}^3 \langle(\delta\mathcal{J}_\alpha)^2\rangle - \frac{1}{2} \sum_{\alpha=1}^3 (\Delta\mathcal{J}_\alpha)^2 \right] k_c^2 e^{-2k_c\langle\mathcal{J}\rangle} \simeq 0 . \quad (18)$$

In order to derive an analytical estimate for the critical infection efficiency from Eq. (18), it is convenient to separate the mean-field contribution,  $k_c^0$ , i.e.  $k_c = k_c^0 + \Delta k$ , and evaluate the value of  $\Delta k$  by expanding Eq. (18) in  $\Delta k \ll k_c^0$ . The zero-order term gives the condition for the critical mean-field value of the infection efficiency,

$$1 - 3e^{-2k_c^0\langle\mathcal{J}\rangle} + e^{-3k_c^0\langle\mathcal{J}\rangle} = 0 , \quad (19)$$

which has the solution  $k_c^0 = -\frac{\ln(1-p_c)}{\langle\mathcal{J}\rangle}$ , where  $p_c = 2 \sin(\pi/18) \simeq 0.347$ .

The next-order terms give an estimate for  $\Delta k$ ,

$$\Delta k \gtrsim \Delta k_3 = \frac{(k_c^0)^2}{2\langle\mathcal{J}\rangle} (V_1 + V_2) , \quad (20)$$

where  $V_1$  and  $V_2$  are defined in the main text by Eqs. (9) and (10).

The estimates of  $\Delta k_1$  and  $\Delta k_2$  for arrangements of type 1 and 2, respectively, can be obtained in a similar way as particular cases of the derivation given above.

## E Mean-field description of complex shapes

In this section, we show how the complex shapes can be approximately represented by effective regular shapes, i.e. effective circles.

In disordered arrangements of type 1, an arbitrary host  $n_i$  from the set of nodes  $\{n\}$  ( $n = 1, \dots, N$ ) is placed at each lattice node  $i$  at uniformly random orientation  $\phi_i$ . The invasion threshold can then be described in terms of a mean-field system in which all the hosts have the same density,  $\langle\rho\rangle(r)$ , where

$$\langle\rho\rangle(r) = \frac{1}{N} \sum_{n=1}^N \int_0^{2\pi} \frac{\rho(\mathbf{r}; n)}{2\pi r} d\phi , \quad (21)$$

defined as the average of the host density  $\rho(\mathbf{r}; n)$  over the  $N$  morphologically different hosts in the ensemble and their orientation. Such averaging eliminates the dependence on the orientation so that  $\langle\rho\rangle(r)$  depends on the radial distance,  $r = |\mathbf{r}|$ , only. By definition, the integral of the density over the 2D plane gives the average ‘‘mass’’ of hosts, i.e. the mass of the effective host in the mean-field system,

$$M = \int_{\mathbb{R}^2} \langle\rho\rangle d^2r . \quad (22)$$

The mean radius of the effective host is then given by

$$\langle r \rangle = \int_{\mathbb{R}^2} r \langle\rho\rangle d^2r . \quad (23)$$

The mean density can be easily obtained by numerical integration of Eq. (21). Fig. 8 shows that the mean density for branching structures appears to decay with radius according to a power law,  $\langle\rho\rangle \sim r^{d_f-2}$  with  $d_f = 1.5 \pm 0.1$  (truncated at large values of  $r$  by an exponential cut-off which accounts for the finite radius of the neurons used here for illustration). This is the expected behaviour for branching

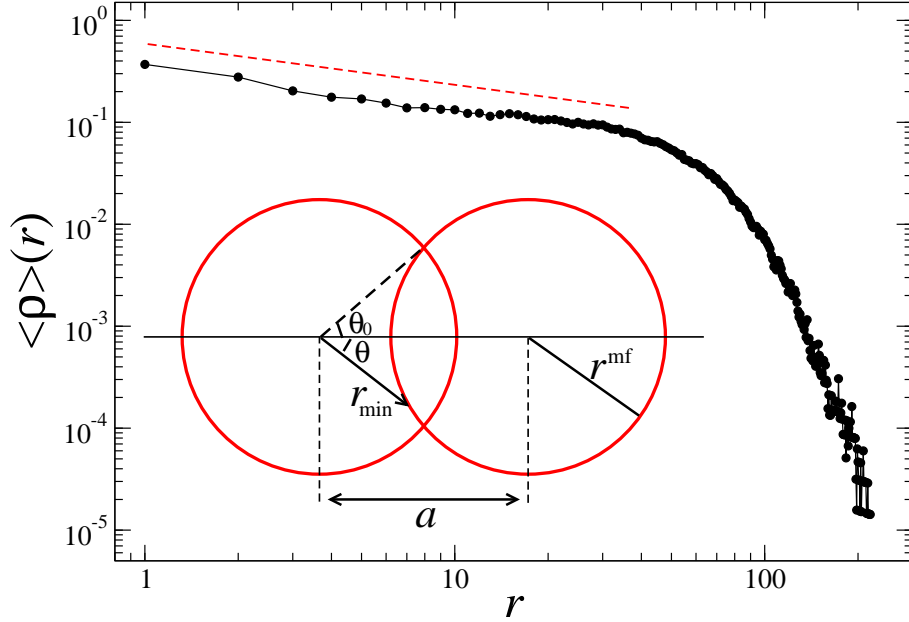


**Figure 8.** Average density for branching structures for disordered arrangements of type 1 versus  $r$ . The dashed line shows a pure power-law behaviour with exponent  $d_f - 2 = -0.5$ . The inset illustrates the overlap of two effective circles of radius,  $r^{\text{mf}}$ , placed at a distance  $a$  apart from each other. The overlap region is defined by the following conditions in polar coordinates  $(r, \theta)$ :  $\{\theta \in [\theta_0, -\theta_0]; r \in [r_{\text{min}}(\theta), r^{\text{mf}}]\}$ .

structures which are non-compact objects and are then characterized by a fractal dimension  $d_f$  smaller than dimensionality  $d = 2$  of the embedding space.

The exponential decay of the mean density at large values of  $r$  can be ignored in the first approximation so that the hosts in the mean-field description can be represented by effective circles of finite radius  $r^{\text{mf}}$  with density,  $\rho^{\text{mf}}(r)$ , given by

$$\rho^{\text{mf}}(r) = \begin{cases} M \frac{d_f (r^{\text{mf}})^{-d_f}}{2\pi} r^{d_f-2}, & r \leq r^{\text{mf}} \\ 0, & r > r^{\text{mf}} \end{cases} \quad (24)$$

The mean-field radius is defined by the following condition,

$$\langle r \rangle = \int_0^{2\pi} d\theta \int_0^{r^{\text{mf}}} r \rho^{\text{mf}}(r) r dr = \frac{d_f}{d_f + 1} r^{\text{mf}}. \quad (25)$$

The value of the mean radius  $\langle r \rangle$  in Eq. (25) can be evaluated for the heterogeneous system using Eq. (23) and thus used for definition of  $r^{\text{mf}}$  to ensure that the mean radius of the effective circle coincides with the mean radius of actual hosts.

The overlap between two effective hosts represented by mean-field circles placed at a distance  $a$  apart from each other (see inset in Fig. 8) is given by Eq. (12) in the main text, i.e by the integral,

$$\mathcal{J}^{\text{mf}} = \left( \frac{M d_f}{2\pi (r^{\text{mf}})^{d_f}} \right)^2 \int_{-\theta_0}^{\theta_0} d\theta \int_{r_{\text{min}}(\theta)}^{r^{\text{mf}}} r^{d_f-1} \left( \sqrt{r^2 + a^2 - 2ar \cos \theta} \right)^{d_f-2} dr, \quad (26)$$

where  $\theta_0$  and  $r_{\min}$  are defined in Fig. 8. If the overlap is small, the above integral can be approximately evaluated by performing an expansion in powers of the linear overlap  $\delta = 2r^{\text{mf}}/a - 1 \ll 1$ , giving

$$\mathcal{J}^{\text{mf}} = \left[ \frac{1}{3} \left( \frac{Md_f}{\pi a} \right)^2 \right] \left( \frac{r^{\text{mf}}}{a} \right)^{-7/2} \delta^{3/2} + \mathcal{O}(\delta^{5/2}). \quad (27)$$

In the system of branching hosts used for illustration in the main text,  $M = 1282.4$  stands for the average number of pixels in the digital images,  $d_f = 1.5 \pm 0.1$ , and  $\langle r \rangle = 50 \pm 5$ . The effective radius is then  $r^{\text{mf}} = 83 \pm 10$  and the approximation to the overlap becomes  $\mathcal{J}^{\text{mf}} \simeq (0.024 \pm 0.008)\delta^{3/2}$ .

## Acknowledgments

FJPR, SNT, FMN and CAG thank BBSRC for funding (Grant No. RG46853). CAG also acknowledges support of a BBSRC Professorial Fellowship. The authors are grateful to Prof. David Schubert (Salk Institute) for comments on disease spreading among neurons. LDFC thanks CNPq (308231/03-1) and FAPESP (05/00587-5) for sponsorship. Part of this work was performed during a Visiting Scholarship of LDFC to St. Catharine's College, University of Cambridge.

## References

- Ascoli, G. A. 2006 Mobilizing the base of neuroscience data: the case of neuronal morphologies. *Nature Rev. Neurosci.*, **7**, 318–324.
- Boender, G. J., Hagenaars, T. J., Bouma, A., Nodelijk, G., Elbers, A. R. W., de Jong, M. C. M. & van Boven, M. 2007 Risk maps for the spread of highly pathogenic avian influenza in poultry. *PLoS Comput Biol*, **3**(4), e71.
- Chen, C.-S., Yao, Y.-C., Lin, S.-C., Lee, Y.-P., Wang, Y.-F., Wang, J.-R., Liu, C.-C., Lei, H.-Y. & Yu, C.-K. 2007 Retrograde axonal transport: a major transmission route of enterovirus 71 in mice. *J. Virol*, **81**, 8996–9003.
- Cook, A. R., Otten, W., Marion, G., Gibson, G. J. & Gilligan, C. A. 2007 Estimation of multiple transmission rates for epidemics in heterogeneous populations. *Proc. Natl. Acad. Sci. USA*, **104**, 20392–20397.
- Cox, J. T. & Durrett, R. 1988 Limit theorems for the spread of epidemics and forest fires. *Stoch. Proc. Appl.*, **30**(2), 171–191.
- Davis, S., Trapman, P., Leirs, H., Begon, M. & Heesterbeek, J. 2008 The abundance threshold for plague as a critical percolation phenomenon. *Nature*, **454**, 634–637.
- Ehrengruber, M. U., Ehler, E., Billeter, M. A. & Naim, H. Y. 2002 Measles virus spreads in rat hippocampal neurons by cell-to-cell contact and in a polarized fashion. *J. Virol*, **76**, 5720–5728.
- Eisinger, D. & Thulke, H.-H. 2008 Spatial pattern formation facilitates eradication of infectious diseases. *J. Appl. Ecol.*, **45**, 415–423.
- Gibson, G. J., Gilligan, C. A. & Kleczkowski, A. 1999 Predicting variability in biological control of a plant-pathogen system using stochastic models. *Proc. Roy. Soc. Ser. B.*, **266**, 1743–1753.
- Gibson, G. J., Kleczkowski, A. & Gilligan, C. A. 2004 Bayesian analysis of botanical epidemics using stochastic compartmental models. *Proc. Natl. Acad. Sci. USA*, **101**, 12120–12124.

- Gilligan, C. A. 2008 Sustainable agriculture and plant diseases: an epidemiological perspective. *Phil. Trans. Roy. Soc. B*, **363**, 741–759.
- González, M. C., Hidalgo, C. A. & Barabási, A.-L. 2008 Understanding individual human mobility patterns. *Nature*, **453**, 779–782.
- Grassberger, P. 1983 On the critical behavior of the general epidemic process and dynamical percolation. *Math. Biosc.*, **63**, 157–172.
- Hinrichsen, H. 2000 Non-equilibrium critical phenomena and phase transitions into absorbing states. *Adv. in Phys.*, **49**, 815–958.
- Isichenko, M. B. 1992 Percolation, statistical topography, and transport in random media. *Rev. Mod. Phys.*, **64**, 961–1043.
- Kenah, E. & Robins, J. 2007 Second look at the spread of epidemics on networks. *Phys. Rev. E*, **76**, 036113.
- Kuulasmaa, K. 1982 The spatial general epidemic and locality dependent random graphs. *J. Appl. Prob.*, **19**, 745–758.
- LaVail, J. H., Topp, K. S., Giblin, P. A. & Garner, J. A. 1997 Factors that contribute to the transneuronal spread of herpes simplex virus. *J. Neuros. Res.*, **49**, 485–496.
- Levin, S. A. & Durrett, R. 1996 From individuals to epidemics. *Phil. Trans R. Soc. Lond. B*, **351**, 1615–1621.
- Liggett, T. M. 1985 *Interacting particle systems*. New York: Springer-Verlag.
- Loewy, A. D. 1998 Viruses as transneuronal tracers for defining neural circuits. *Neurosc. Biobehav. Rev.*, **22**(6), 679–684.
- Marro, J. & Dickman, R. 1999 *Nonequilibrium phase transitions in lattice models*. Cambridge: Cambridge University Press.
- Miller, J. C. 2007 Epidemic size and probability in populations with heterogeneous infectivity and susceptibility. *Phys. Rev. E*, **76**(1), 010101. (doi:10.1103/PhysRevE.76.010101)
- Murray, J. D. 2002 *Mathematical biology. i. an introduction*. Springer, 3rd edn.
- Newman, M. E. J. 2002 Spread of epidemic disease on networks. *Phys. Rev. E*, **66**, 016128.
- Ódor, G. 2004 Universality classes in nonequilibrium lattice systems. *Rev. Mod. Phys.*, **76**, 663–724.
- Oztaş, E. 2003 Neuronal tracing. *Neuroanatomy*, **2**, 2–5.
- Samuel, M. A., Wang, H., Siddharthan, V., Morrey, J. D. & Diamond, M. S. 2007 Axonal transport mediates west nile virus entry into the central nervous system and induces acute flaccid paralysis. *Proc. Natl. Acad. Sci. U.S.A.*, **104**(43), 17140–17145.
- Sander, L., Warren, C. P. & Sokolov, I. M. 2003 Epidemics, disorder, and percolation. *Physica A*, **325**, 1–8.
- Sander, L., Warren, C. P., Sokolov, I. M., Simon, C. & Koopman, J. 2002 Percolation on heterogeneous networks as a model for epidemics. *Math. Biosc.*, **180**, 293–305.

- Soriano, J., Martínez, M. R., Tlustý, T. & Moses, E. 2008 Development of input connections in neural cultures. *Proc. Natl. Acad. Sci. USA*, **105**, 13 758–13 763.
- Sornette, D. 2000 *Critical phenomena in natural sciences*. Springer Series in Synergetics. Berlin: Springer Verlag.
- Stauffer, J. & Aharony, A. 1994 *Introduction to percolation theory*. Washington, D.C.: Taylor and Francis, 2nd edn.
- Sykes, M. F. & Essam, J. W. 1964 Exact critical percolation probabilities for site and bond problems in two dimensions. *J. Math. Phys.*, **5**, 1117–1127.
- Truscott, J. E. & Gilligan, C. A. 2003 Response of a deterministic epidemiological system to a stochastically varying environment. *Proc. Natl. Acad. Sci. USA*, **100**, 9067–9072.
- Volz, E. 2008 Susceptible-infected-recovered epidemics in populations with heterogeneous contact rates. *Eur. Phys. J. B*, **63**, 381–386.